Jordan Journal of Physics

ARTICLE

Comparative Analysis of the Effect of Polystyrene Coating on the Field Emission Characteristic of Tungsten and Carbon Fiber Emitters

Marwan S. Mousa^a, Ildiko Tulbure^{b,c,d}, Moneeb T. M. Shatnawi^e, Saleh H. Fawaeer^f, Alexandr Knápek^g, Vlasta Sedláková^h, M-Ali H. Al-Akhrasⁱ, Mo'tasem Alabth^e, Mohmmad M. Allaham^{g,h}, Ammar Al Soud^{f,h}, Samer I. Daradkeh^f, Kipkurui Ronoh^{f,j}, Wala' M. Al-Qaisi^f and Dinara Sobola^{f,i,j}

Doi: https://doi.org/10.47011/18.3.8

Received on: 22/02/2024; Accepted on: 02/06/2024

Abstract: Achieving high initial emission currents at relatively low operating voltages is essential for field electron emission sources utilized in equipment reliant on focused electron beams. Coating these emitters with a dielectric layer has the potential to enlarge their effective emission region, thereby increasing the initial emission current value while simultaneously reducing the operating voltage. This study compares and contrasts the effects of a dielectric polystyrene coating on field electron emission characteristics, drawing on two investigations of polystyrene-coated emitters. The study provides a brief analysis of the field electron emission characteristics obtained from carbon fiber and tungsten emitters, both prepared using electrochemical etching and subsequently coated with polystyrene. Both studies are thoroughly reviewed and contextualized, emphasizing the advantageous attributes of this emitter type. The focus of the study lies in the currentvoltage characteristic, Murphy-Good analysis plot, and field electron emission images obtained from both emitters, with particular attention to how the coating influences emissivity. The investigation into the emission characteristics of coated tungsten indicates a significant improvement over coated carbon fiber emitters, with performance enhanced several times.

Keywords: Carbon fiber emitter, Dielectric polystyrene coating, Field electron emission, Murphy-good plot, Tungsten emitter.

Corresponding Authors:Marwan S. MousaEmail: m.mousa@jadara.edu.joSaleh H. FawaeerEmail: saleh.hekmat@ceitec.vutbr.cz

^a Department of Renewable Energy Engineering, Jadara University, Irbid 21110, Jordan.

^b University "1 Decembrie 1918", Alba Iulia 510009, Romania.

^c Technical University of Cluj-Napoca, Cluj-Napoca 400114, Romania.

^d Clausthal University of Technology, Clausthal-Zellerfeld 38678, Germany.

^e Department of Physics, The University of Jordan, Amman 11942, Jordan.

^f Central European Institute of Technology, Brno University of Technology, Purkyňova123, Brno 612 00, Czech Republic.

g Institute of Scientific Instruments of Czech Academy of Sciences, Královopolská 147, Brno 612 00, Czech Republic.

h Department of Physics, Faculty of Electrical Engineering and Communications, Brno University of Technology, Technická 2848/8, Brno 616 00, Czech Republic.

ⁱ Department of Physics, Jordan University of Science and Technology, Irbid 22110, Jordan.

^j Academy of sciences ČR, Institute of Physics of Materials, Žižkova 22, Brno 616 00, Czech Republic.

1. Introduction

In recent years, the rapid advancement of nanofabrication technology [1-3] has reignited interest in nano-field electron emission (FEE) particularly sharp-point emitters emitters, designed for high current density applications [4–7]. Cold field electron emission from a metal source coated with a dielectric layer has attracted considerable attention due to its relevance for electron-beam-based equipment. applications require a high-quality source of free electrons that is intense and capable of providing high current density while operating in less-thanideal vacuum conditions [8-11]. To meet these demands, experimental coated FEE-emitters based on sharp emitters such as tungsten (W) [12, 13], molybdenum (Mo) [14], tantalum (Ta) [1], and carbon fibre (CF) [15], featuring a metal oxide-dielectric structure, have emerged as promising candidates [8].

The advantages of coated FEE sources are noteworthy: (I) Minimal demagnification is required to achieve a probe with a diameter as small as 1 nm, thanks to the small virtual source size starting from a few nanometers [2, 3]. (II) The presence of minimal energy spread allows operation at low accelerating Consequently, exceptionally sharp, high-contrast images can be obtained without inducing considerable damage. (III) The coating layer facilitates operation in a relatively low-quality vacuum ($\leq 10^{-6}$ Pa), thereby mitigating ionbombardment and the sorption of residuals on the emitter's surface. Maintaining a lower vacuum level also enables quicker sample manipulation [9, 13].

The need for a deeper comprehension of FEE phenomena and the advancement of field electron emission theories for dielectric-coated emitters serve as the driving force for further investigation into the behavior of coated emitters [4, 16–18]. Therefore, numerous comprehensive experimental studies have been conducted to simulate this type of FFE-tips by fabricating and characterizing various kinds of sharp emitters to investigate their FEE-behavior before and after covering with a dielectric material. These studies revealed that coated FEE-tips exhibit several promising operational properties compared to the performance of well-known uncoated emitters [11, 12, 15, 19, 20]. Additionally, certain dielectric coatings enhance FEE at low fields

(<V/nm) when applied to emitter surfaces [9, 12, 15, 19, 21]. Indeed, cold field electron emission occurs once an electric field is applied to the coated emitter, resulting in a higher emission current at significantly lower voltage compared to the uncoated emitter. Cycling of the voltage yields reproducible current-voltage (I – V) characteristics with enhanced stability and brighter spot [22–27].

Following these promising findings, two experimental studies were conducted on two different kinds of electron sources coated with polystyrene (PS) dielectric material [26, 27]. In these studies, a thin coat of PS material was applied to CF and W emitters with different thicknesses (\leq 350nm). The objective was to evaluate the FEE characteristics and capabilities of these coated emitters as field-electron emission sources, studying the effect of PScoating on their emission properties. The Murphy-Good (MG) plot was employed as an advanced method to analyze the acquired I - Vdata, providing a more precise characterization of emitter behavior. This plot serves as a graphical representation of the MG equation, which was developed to characterize emitter behavior based on an advanced mathematical understanding of Fowler-Nordheim theory [16, 17, 28-30]. Both studies presented results from FEE sources, specifically CF and W emitters, both before and after being coated with PS. Their findings demonstrated that coated emitters exhibit several promising properties compared to uncoated emitters. These coated emitters showed significant enhancements in the emission process, including higher emission current values, lower threshold voltages, brighter emission images, and more intense electron beams [26, 27].

This study provides a brief analysis of the field emission behavior of two experimental emitters: PS-coated CF and W emitters, as presented in two distinct works. By compiling data from their I – V characteristic curves, MG analysis plots, FEE images, and scanning electron micrographs, this study investigates and elucidates the similarities and differences in how PS coatings influence the performance of CF versus W emitters.

2. Materials and Methods

2.1. Emitter Fabrication

In the first study, experiments were carried out using polyacrylonitrile VPR-19 carbon fibre (7 µm in diameter), while in the second study, high-purity polycrystalline tungsten wire with a diameter of 0.1 mm was used. These choices were made due to the distinctive features of CF and W, such as their high melting points (3970 K for CF and 3650 K for W), high work function (4.95 eV for CF and 4.55 eV for W), as well as their high hardness, strength, and heat resistance at elevated temperatures [12, 13, 15].

For the fabrication of FEE-emitters, they are typically shaped into sharp emitters with an emitter-apex radius of a few nanometers [3, 4]. In both works [26, 27], the sharp emitters used as a substrate for the PS-coating layer were fabricated using the same method based on electrolytic etching [12, 15]. A solution of 0.1 molar sodium hydroxide (NaOH) was employed to etch the CF [25], while a solution of 2 molar NaOH was used to etch the W wire [23]. The etching process of the emitters was controlled by selecting an appropriate initial etching current to produce sharp emitters on the solution surface. Approximately 35 µA of current was applied for CF etching, while 4 mA was applied for W-wire etching [24]. Following the etching process, the samples (i.e., the etched tips) were cleaned in water for a few minutes, utilizing a sonicator to remove contaminants arising from the electrolytic etching [9].

Since polystyrene (C₈H₈)_n has a high melting point [3] and a low work function (4.22 eV) [31], its solution has been used as a dielectric coating for etched tips. In both works, PS-pellets (as the solute) and toluene (as the solvent) were used to prepare a PS-coating solution with different concentrations. The covering process in both works involved dipping the emitter into the PS-coating solution and ensuring its apex was coated with a layer as homogeneous as possible. In the first work, the CF-emitter was dipped several times into a solution of 0.16 g/mL PS, forming a layer that was approximately 50-75 nm thick, while in the second work, the W-emitter was also dipped

several times into a solution of 0.8 g/mL PS, resulting in a 100–150 nm thick layer [26, 27]. The variation in coating thickness was due to differences in solution concentration and the number of dipping cycles.

In both works, the emitter was subsequently subjected to a curing cycle, and the PS-layer underwent a glass transition, transforming into a hard and relatively brittle "glassy" material [9]. In the first work, the CF-emitter was baked directly in the FEE-vacuum chamber during the degassing procedure, whereas in the second work, the W-emitter was cured in an electric furnace. The curing process involved two stages: heating for 10 minutes at 100 °C to remove solvents, followed by another 10 minutes at 120 °C to complete the curing process [26, 27].

Figures 1 and 2 show the emitters from both works using scanning electron microscopy (SEM), which was employed in both cases before and after PS coating. This was done to determine the radius of the FEE-tip apex resulting from the etching process, and subsequently followed by the coating process. By subtracting these two values, the thickness of the dielectric PS-coating layer formed on top of the etched tip could be determined [23, 25]. Additionally, the SEM images reveal the slight difference in surface contrast between the dielectric PS-coating layer and the core tip, providing insights into the fine structure of the composite emitter.

Since it is a complementary method and provides different information about the etched tip and the coating layer, Fig. 1 presents SEM-images of the first and second carbon fibre samples (labelled as CF¹ and CF²) with a tip apex radius of 41.3 and 63.4 nm, respectively, (a) before and (b) after coating with a dielectric PS-layer of 92.5 and 54.3 nm thickness, respectively [26]. Similarly, SEM-images of the first and second tungsten samples (labelled as W¹ and W²) with a tip apex radius of 161 and 170 nm, respectively, are shown in Fig. 2: (a) before and (b) after coating with a dielectric PS-layer of thickness 142 and 105 nm, respectively [27].

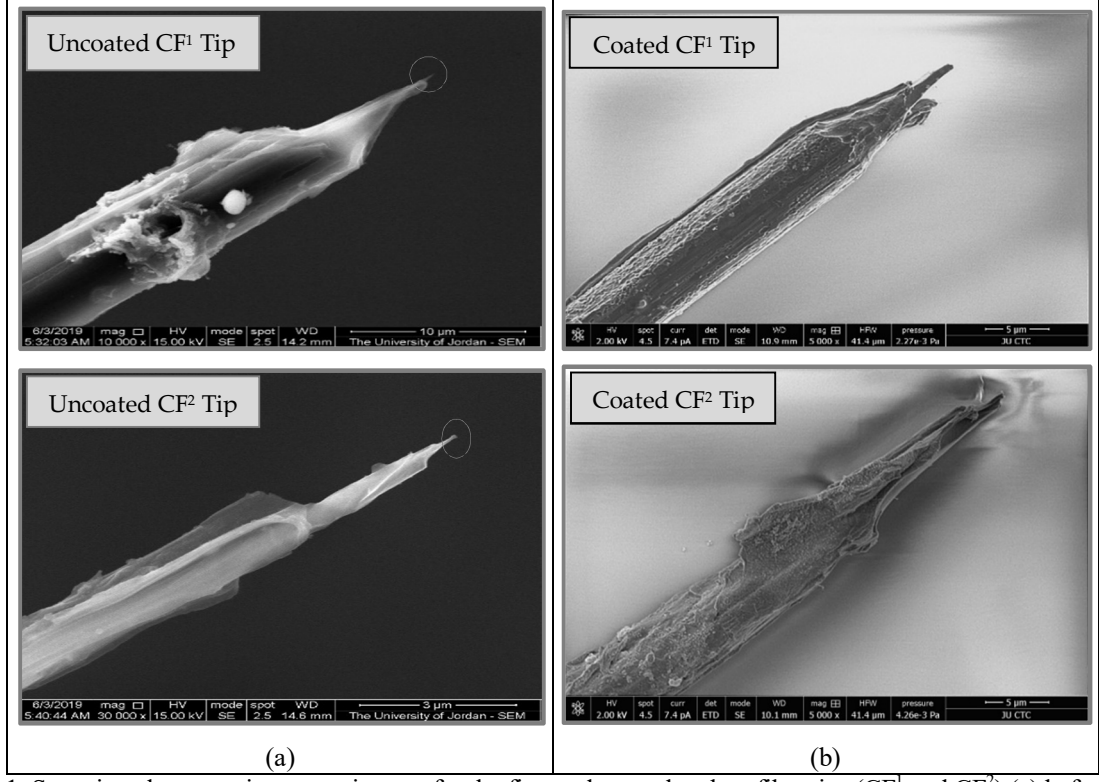


FIG. 1. Scanning electron microscope images for the first and second carbon fibre tips (CF¹ and CF²) (a) before and (b) after polystyrene coating [26].

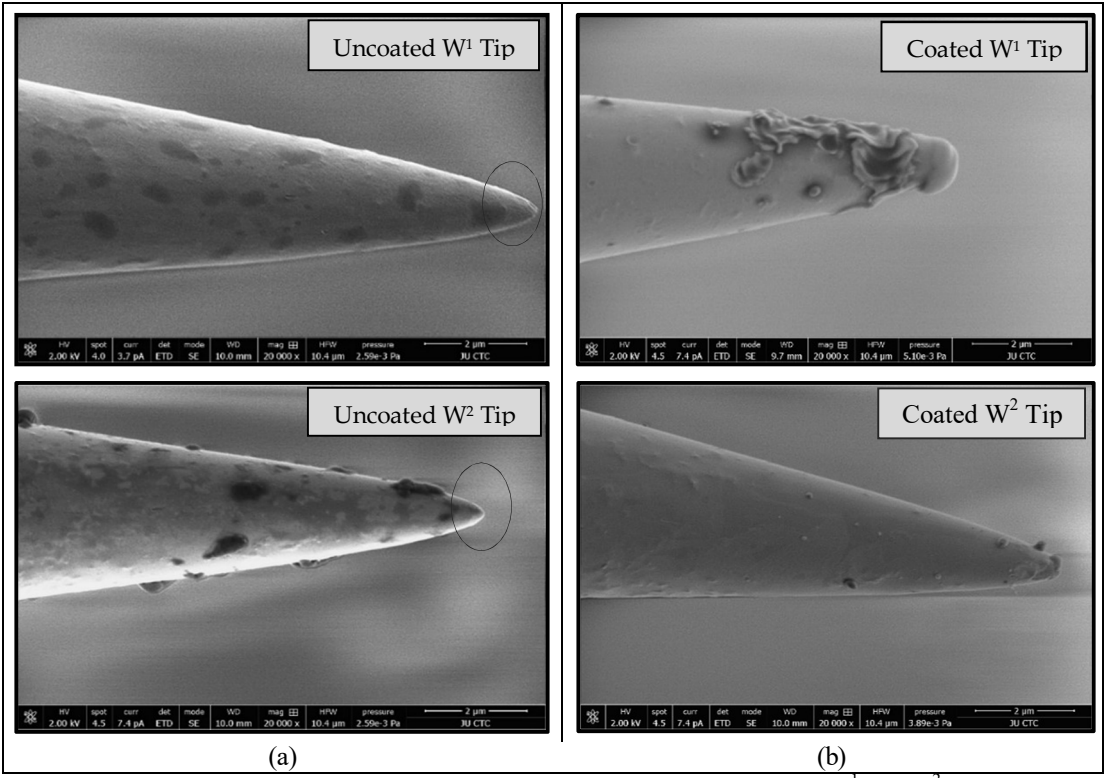


FIG. 2. Scanning electron microscope images for the first and second tungsten tips (W¹ and W²) (a) before and (b) after polystyrene coating [27].

2.2. Analytical Facility

In both FEE studies, the most important results obtained from coated emitters were the

I - V characteristics [8, 19, 22–25], which were analyzed by applying analytical MG plots [16, 17, 28]. The I - V data were acquired utilizing a home-built field emission microscope (FEM).

Inside a high-vacuum chamber, the emitter (acting as a cathode) was positioned 1 cm away from a phosphorus screen (serving as an anode), which was grounded by picometers to measure the emission current. The emitter was connected to a high-voltage power source to induce electron emission after applying a voltage across the emitter. The specific setup and measurement procedures were described in detail in [26, 27]. The summary provided in this work pertains to investigations conducted under high vacuum conditions at a pressure ranging from 10⁻⁶ to 10⁻⁸ mbar. This vacuum was achieved inside the chamber with the help of a slow baking process of the system at 140-170 °C, followed by a rapid cooling process with liquid nitrogen to maintain the vacuum for as long as possible [26, 27]. This high vacuum is crucial to diminish the ion-bombardment rate of gas molecules on the emitter surface and to keep it from being damaged [9,20].

3. Results and Discussion

This part shows the results acquired from the CF and W-tips before and after PS coating, highlighting similarities and differences in their FEE characteristics. These findings encompass the I-V characteristics and FEM images [26, 27].

3.1. Analysis of the Emission Characteristics Obtained from Coated Emitters

3.1.1 Current-voltage (I - V) Characteristics

The current-voltage curve was used to model the behavior of the FEE emitter during operation. Additionally, the MG plot was used to characterize the emitter behavior by interpreting the I — V data and analyzing it graphically. The rationale behind using the MG plot was to derive an approximate linear relationship from the practical FEE data. Improvements in emitter behavior after coating were assessed by the extent to which the linearity of the data was enhanced [16, 28, 30].

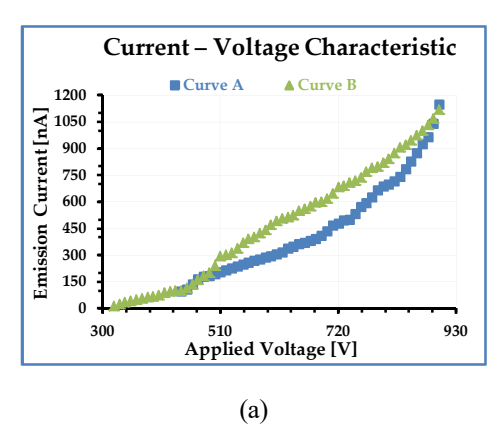
3.1.1.1 Polystyrene—Coated Carbon Fibre Emitters

For the first and second uncoated CF samples presented in Fig. 1(a), emission was

observed to initiate after applying an initial operating voltage across the emitter at 440 V and 590 V, respectively. This resulted in an initial emission current of 96 nA and 41 nA, respectively. With increasing applied voltage, the I–V characteristics (curve A) for the uncoated CF1 and CF2 emitters were obtained, as shown in Figs. 3(a) and 4(a), respectively. These curves extended over a wide voltage range, up to 900 V and 910 V, with current values of 1.15 μ A and 1.74 μ A, respectively. When the voltage applied across the emitter was lowered to threshold values of 320 V and 360 V, the FEE behavior followed a trend like curve B, as shown in Figs. 3(a) and 4(a), for the uncoated-CF¹ and CF²-samples, respectively.

Murphy-Good plots of the current-voltage characteristics (curves A and B) for the uncoated-CF-samples were found to be approximately linear in the region of emission currents < 10⁻⁷ A, as shown in Figs. 3(b) and 4(b) for the uncoated CF¹ and CF² emitters, respectively. However, significant linear deviations were observed in the region with higher emission current values. This property is known and related to this type of emission process [23–25].

In Figs. 5(a) and 6(a), curve A represents the current-voltage characteristics of the first and second CF samples coated with 92.5 and 54.3 nm of PS, respectively, as shown in Fig. 1(b). Compared with curve A in Figs. 3 and 4, the initial operating voltages applied across the PScoated CF¹ and CF² emitters decreased slightly to 350 V and 540 V, respectively, while their initial emission current values increased to 81 nA and 102 nA. Moreover, an additional appeared, shifting the I - Vhysteresis characteristics slightly towards higher emission current values when the applied voltage across the PS-coated CF¹ and CF² emitters was increased to the range of 900-950 V, with an emission current value of 1880 nA. When the voltage applied across the PS-coated CF¹ and CF² emitters was lowered to threshold values of 330 and 400 V, respectively, their FEE behavior followed a pattern similar to curve B, as shown in Figs. 5(a) and 6(a).



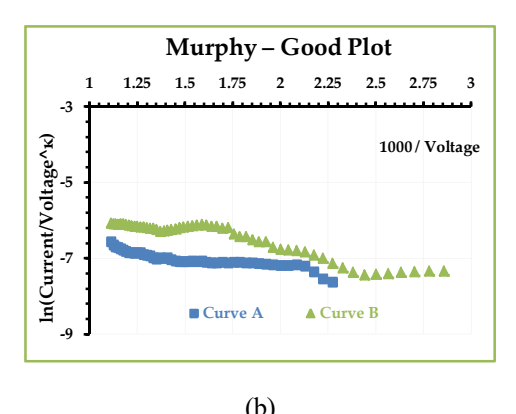
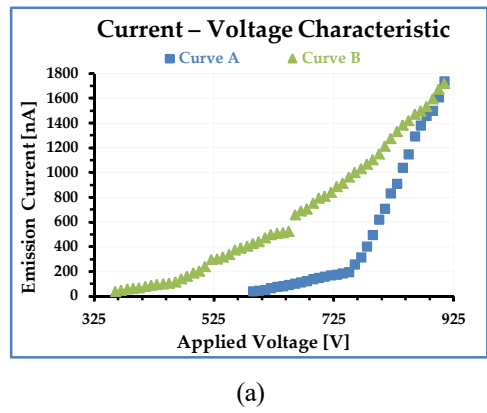


FIG. 3. Current-voltage characteristic of the uncoated CF¹ emitter with an apex radius of 41.3 nm: (a) emission behavior during increasing (curve A) and decreasing (curve B) voltage cycles; (b) corresponding Murphy–Good plots for the same tip under both cycles.



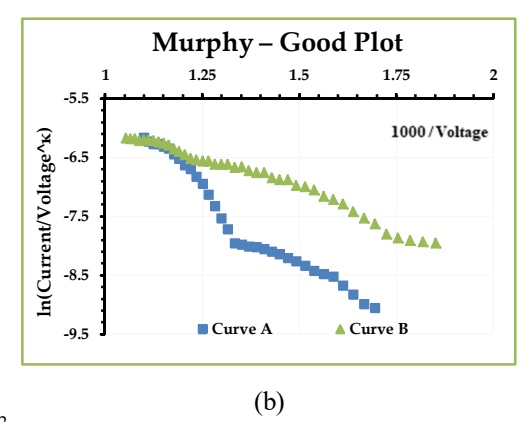
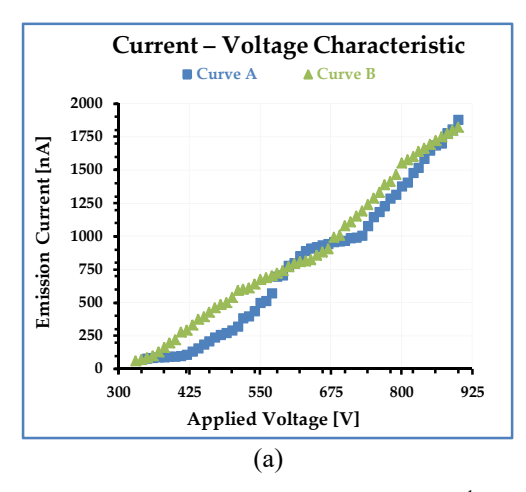


FIG. 4. Current-voltage characteristic of the uncoated CF² emitter with an apex radius of 63.4 nm: (a) emission behavior during increasing (curve A) and decreasing (curve B) voltage cycles; (b) corresponding Murphy–Good plots for the same tip under both cycles.

Figures 5(b) and 6(b) display the Murphy-Good plots of the current-voltage data for the PS-coated CF¹ and CF² emitters, respectively. Comparing the MG-plot of the current-voltage characteristics of the uncoated and coated CF samples reveals a noticeable difference in the low-field region. Specifically, the slopes of the approximately linear relations are slightly lower for the PS-coated emitters (Figs. 5 and 6) than for the uncoated ones (Figs. 3 and 4). This reduction in slope suggests that the coating layer enhanced the effective emissive area of the emitters by lowering the work function of the composite coated tips. As a result, a lowerpotential Schottky-Nordheim barrier was formed at reduced applied fields. Once this barrier was

sufficiently suppressed by the applied voltage, electrons from states near the Fermi level could tunnel through, generating a denser electron beam with higher emission current at a lower extraction voltage. Consequently, the FEE characteristics of the coated emitters were significantly improved compared with those before coating [12, 21]. Similar effects have been reported and discussed in previous works [9, 22–25].To provide perspective on the variability in the FEE performance of this type of CF-tip, Table 1 summarizes the compiled current-voltage data for CF¹ and CF² tips before and after coating with PS.



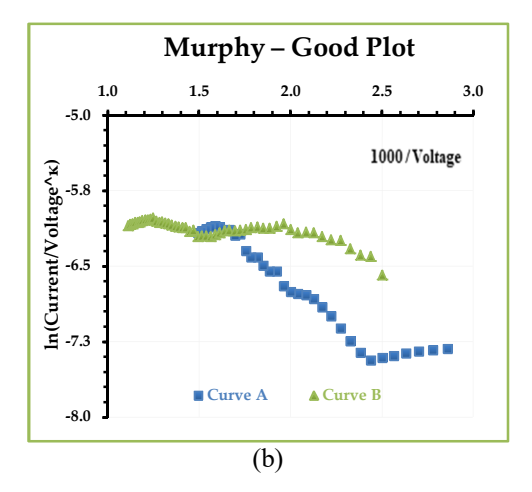
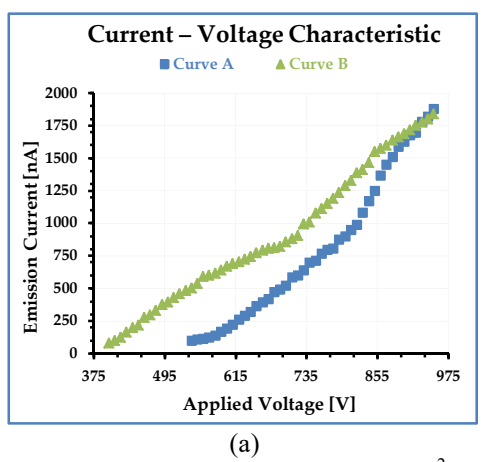


FIG. 5. Current-voltage characteristic of a CF¹ emitter with a tip radius of 41.3 nm coated with a 92.5 nm PS layer during (a) increasing (curve A) and decreasing (curve B) cycles. (b) Murphy–Good plot of the same tip for the increasing and decreasing cycles.



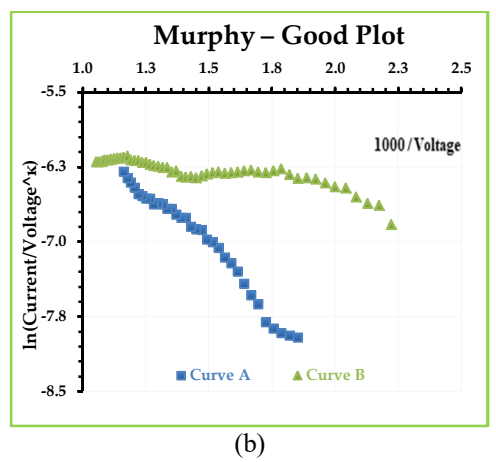


FIG. 6. Current-voltage characteristic of a CF² emitter with a tip radius of 63.4 nm coated with a 54.3 nm PS layer during (a) increasing (curve A) and decreasing (curve B) cycles. (b) Murphy–Good plot of the same tip for the increasing and decreasing cycles.

TABLE 1. Compiled current-voltage data for CF¹ and CF² tips before and after they were covered with PS.

Sample	Radius	Cycle	Voltage range	Emission current
Sumple	(nm)		(V)	(nA)
Uncoated CF ¹ – tip	41.3	Increasing Voltage	440 - 900	96-1151
Oncoated Cr — tip	41.5	Decreasing Voltage	900 - 320	1120 – 13
CF ¹ – tip coated with a PS layer 92.5 nm	133.8	Increasing Voltage	350 - 900	81 - 1880
thick		Decreasing Voltage	900 - 330	1820 - 63
Uncoated CF ² – tip	63.4	Increasing Voltage	590 – 910	41 – 1741
Oncoated Cr — tip	03.4	Decreasing Voltage	910 - 360	1770 - 38
$\overline{\text{CF}^2}$ – tip coated with a PS layer 54.3 nm	117.7	Increasing Voltage	540 – 950	102 - 1880
thick	11/./	Decreasing Voltage	950 - 400	1840 – 79

3.1.1.2 Polystyrene—Coated Tungsten Emitters

For the first and second uncoated W samples presented in Fig. 2(a), their current—voltage measurements are represented in Figs. 7 and 8, respectively. Part (a) shows the I-V characteristics, while part (b) displays the MG-plot of the I-V data. From curves A and B

of the uncoated W emitters, it can be observed that their FEE behavior follows a somewhat similar trend to that of the uncoated CF emitter curves, although they cover a wider range of extraction voltages. As shown in Figs. 7 and 8, emission for the uncoated W1 and W2 emitters began at initial operating voltages of 750 and

1050 V, respectively, with emission current values of 30 and 1 nA. Subsequently, when the voltage applied across the emitters was increased to 2000 and 2150 V, the emission current values reached 4000 and 800 nA, respectively. Upon reducing the applied voltage across the uncoated W¹ and W² emitters to threshold values of 900 and 1000 V, respectively, the FEE behavior followed a trend similar to curve B, as shown in Figs. 7(a) and 8(a), respectively.

The Murphy-Good plots in Figs. 7(b) and 8(b) indicate that the I-V data for the uncoated W samples followed almost the same

Current – Voltage

Curve

Curve

A

Curve

Curve

A

Curve

Curve

A

Curve

Applied Voltage (V)
(a)

1550

2075

approximately linear relation as that of the MG plots for the uncoated CF samples, with a slight difference in the slope value. This slight difference in the emission I – V characteristics for both emitters is mainly due to the different chemical structure (CF vs. W), different work function, and tip sharpness, as they all influence and contribute to the formation of a low-potential Schottky-Nordheim barrier, which in turn affects the field electron emission characteristics from the emitter. Several studies have explained these effects on emissivity in more detail [8, 22–25].

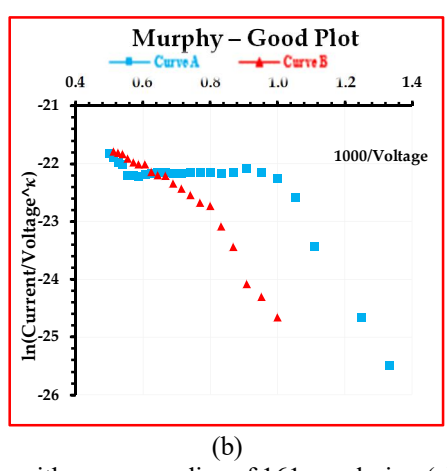
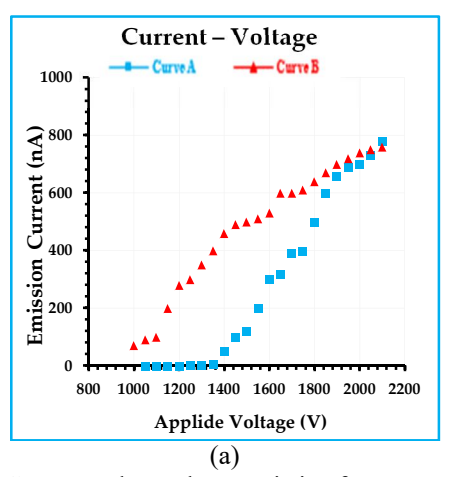


Fig. 7. Current-voltage characteristic of an uncoated W¹ tip with an apex radius of 161 nm during (a) increasing (curve A) and decreasing (curve B) cycles. (b) Murphy–Good plot for the same tip during the increasing and decreasing cycles.



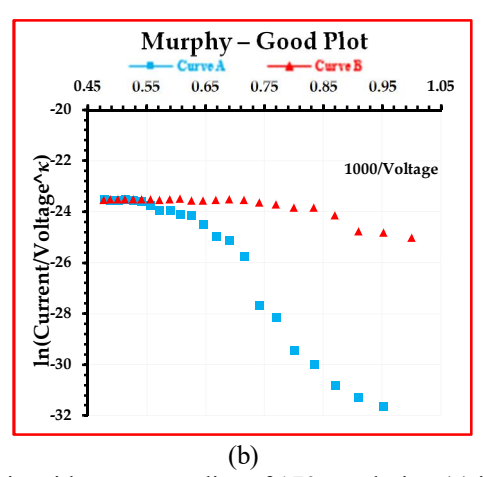


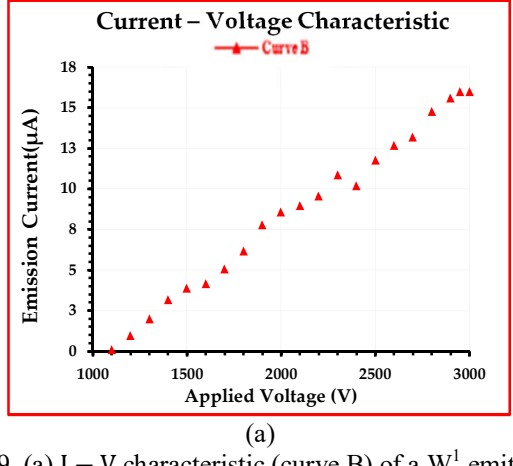
Fig. 8. Current-voltage characteristic of an uncoated W² tip with an apex radius of 170 nm during (a) increasing (curve A) and decreasing (curve B) cycles. (b) Murphy–Good plot for the same tip during the increasing and decreasing cycles.

For the first and second W samples coated with a PS layer with thicknesses of 142 and 105 nm, as presented in Fig. 2(b), a distinctive behavior was observed compared to the PS-coated CF emitters when the voltage applied across the coated W tip was increased. This behavior included the phenomenon known as the

'switch-on'. The 'switch-on' refers to the sudden appearance of a high emission current, referred to as the 'saturation' current (I_{SAT}), usually in microamperes, at a certain voltage termed the 'switch-on voltage' (V_{SW}) during voltage rampup [11–13, 32]. In this case, the initiation of field electron emission was noticed after applying a

switch-on voltage across the PS-coated W^1 and W^2 emitters at 3000 and 3700 V, respectively, which produced saturation current values of 16 and 18 μ A, respectively, and was maintained at lower voltages. After the current stabilized, lowering the voltage applied across the emitter to

a threshold voltage of 1100 and 500 V produced the I-V characteristic (curve B) and the MG analysis-plot for this case, as shown in Figs. 9 and 10 for the PS-coated W^1 and W^2 emitters, respectively.



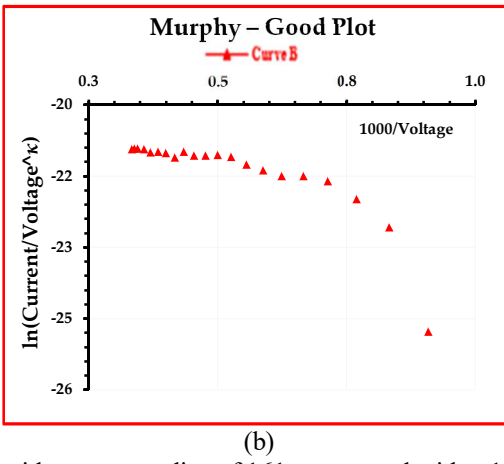
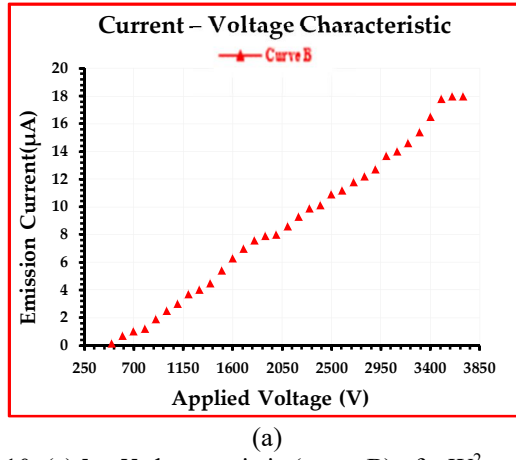


Fig. 9. (a) I – V characteristic (curve B) of a W¹ emitter with an apex radius of 161 nm, coated with a 142 nm thick PS layer. (b) Corresponding MG plot during the first voltage decrease.



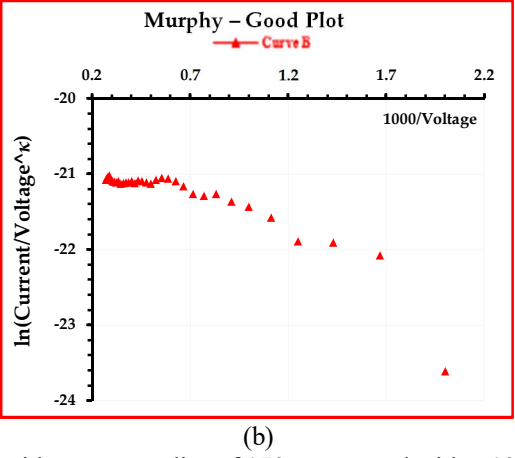


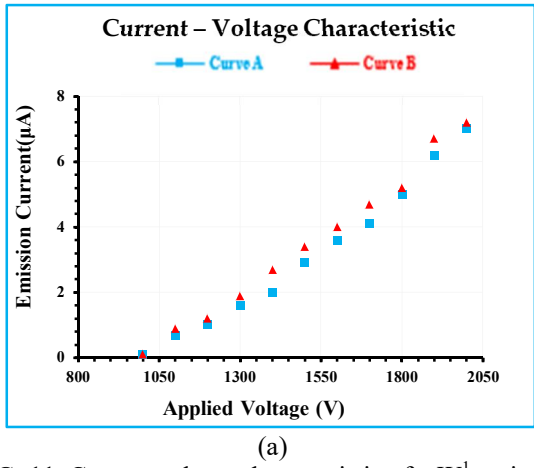
Fig. 10. (a) I – V characteristic (curve B) of a W² emitter with an apex radius of 170 nm, coated with a 105 nm thick PS layer; (b) corresponding MG plot during the first decreasing voltage cycle.

Then, a complete voltage cycle was applied across the coated W samples to produce the I - V characteristics for their FEE behavior during operation, as shown in Figs. 11(a) and 12(a) for the PS-coated W¹ and W² emitters, respectively. Compared to the uncoated W emitters (curve A in Figs. 7 and 8), the PScoated W1 and W2 samples exhibited higher initial emission current values of 100 and 900 nA at applied voltages of 1000 and 500 V, respectively. It is also evident that an additional causing hysteresis occurred, the characteristic to shift slightly towards higher emission current values when the applied voltage across the PS-coated W1 and W2 samples was increased to 2000 and 2500 V, resulting in emission current values of 7000 and 11000 nA, respectively. When lowering the voltage applied across the PS-coated W¹ and W² emitters to a threshold voltage, the FEE performance followed a trend similar to curve B, as shown in Figs. 11(a) and 12(a), respectively.

In the Murphy-Good plot of the current-voltage data for the PS-coated W^1 and W^2 emitters shown in Figs. 11(b) and 12(b), respectively, a certain similarity can be observed with the MG-plot shown in Figs. 5(b) and 6(b). This similarity arises from the fact that the I-V data obtained from the PS-coated W emitter followed the same approximately linear relation with lower slope values than the uncoated W

emitter, similar to the effect observed with the coated CF emitter. This implies that the effect of the PS-coating layer on FEE behavior for both coated emitters was the same. However, comparing the MG plots of the PS-coated W emitters with those of the PS-coated CF emitters also shows a difference in slope values. This difference arises primarily from variations in

chemical structure (PS-coated CF vs. PS-coated W), work function, and coating thickness, all of which influence the field electron emission characteristics. These effects have been discussed in detail in previous studies [9, 22, 23]. Table 2 provides a perspective on the variability in FEE performance observed for this type of W-tip.



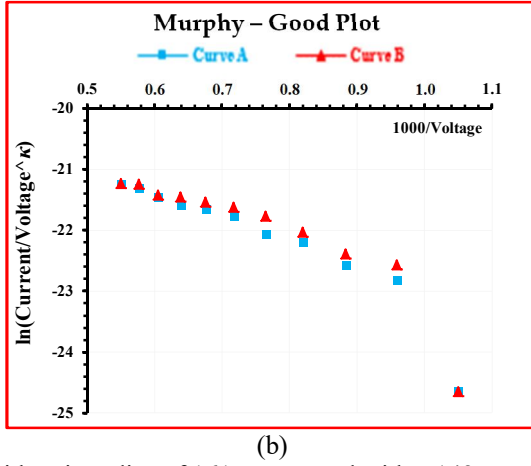
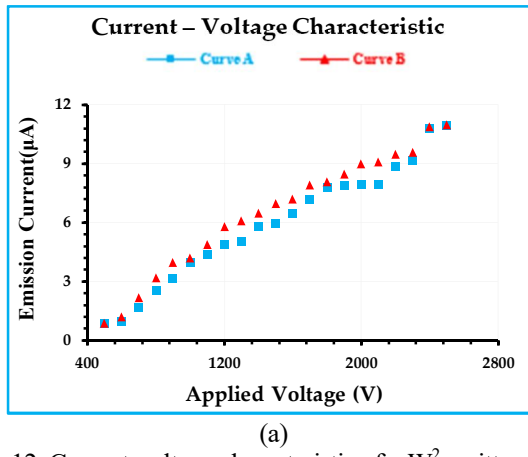


FIG. 11. Current-voltage characteristic of a W¹ emitter with a tip radius of 161 nm, coated with a 142 nm thick PS layer, during (a) increasing (curve A) and decreasing (curve B) voltage cycles. (b) Murphy–Good plot for the same emitter showing the corresponding increasing and decreasing cycles.



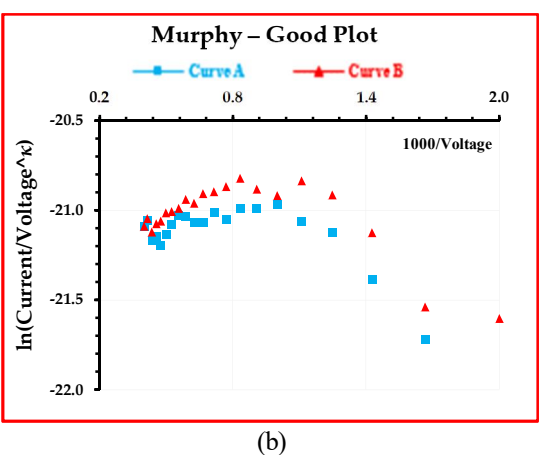


FIG. 12. Current-voltage characteristic of a W² emitter with a tip radius of 170 nm covered by a 105 nm thick PS layer during (a) increasing (curve A) and decreasing (curve B) cycles. Murphy–Good plot for the same emitter during (b) the increasing and decreasing cycles.

TABLE 2. Compiled data from current–voltage measurements for W¹ and W² tips, before and after they were covered by PS.

	Radius - (nm)	First Decreasing Cycle			Voltage	Emission	
Sample		Switch-on	Saturated	Cycle	Range (V)	Current (nA)	
		Voltage	Emission Current				
Uncoated W ¹	161	No "switch-on" phenomenon		Increasing Voltage	750 - 2000	30 - 4000	
tip		No switch-on phenomenon		Decreasing Voltage	1950 - 900	4000 - 60	
W ¹ tip coated		Voltage Range:	Current Range:	Ingranging Valte	22 1000 2000 100 7000		
with 142 nm	303	303 (3 – 1.1) KV	$(16-0.1) \mu A$	Increasing Voltage 1000 – 2000 100 – 7000 Decreasing Voltage 2000 – 1000 7200 – 100			
PS layer		3 KV 16 μA		Decreasing voltage 2000 – 1000 /200 – 100			
Uncoated W ²	170	No "quitab or	" nhanamanan	Increasing Voltage	1050 - 2150	1 - 800	
tip		No "switch-on" phenomenon		Decreasing Voltage	2100 - 1000	760–70	
W ² tip coated		Voltage Range:	Current Range:	Ingressing Voltage 500 2500 000 11000			
with 105 nm PS	275	$(3.7-0.5) \ KV \ (18-0.12) \ \mu A$		Increasing Voltage 500 – 2500 900 – 11000 Decreasing Voltage 2500 – 500 11000 – 900			
layer		3.7 KV	18 μΑ	Decreasing voltage 2500 – 500 11000 – 500			

3.1.2 Emission Images Characteristics

The emission image that appears on the FEM phosphor screen, which is used to display the field electron emission shape, is also referred to as an emission pattern due to its geometric arrangement. In both studies, a photograph of the FEE image was captured to analyze the emission pattern from the uncoated and coated emitters. This analysis aimed to investigate the effect of coating on the FEE characteristic by comparing the differences between the two patterns.

3.1.2.1 Polystyrene— Coated Carbon Fibre and Tungsten Emitters

Figures 13(a) and 13(b) show the emission images of the uncoated CF¹ and CF² emitters, while Figs. 13(c) and 13(d) show those of the corresponding PS-coated emitters. Figures 14(a) and 14(b) present the uncoated W¹ and W² emitters, and Figs. 14(c) and 14(d) show the PScoated emitters. All images were obtained during the voltage-up cycle corresponding to the I-V characteristic (curve A) discussed in the subsections on PS-coated CF and W emitters [26, 27]. The FEE images obtained from the uncoated CF and W emitters, shown in Figs. 13(a) and 14(c) display the active emission region on the emitter surface. The emission appears as a multicenter spot, where the densely packed centers within the spot (i.e., sharper regions of the tip surface) have a lower work function than the surrounding areas (i.e., less sharp, atomically rough regions). As a result,

bright centers appear against a dimmer background.

By contrast, the FEE images of the PS-coated emitters in both studies, presented in Figs. 13(b) and 14(d) show a concentric emission area, appearing as a single, highly bright central spot. Unlike the uncoated emitters, which exhibit multiple bright spots due to a background structure, the coated emitters display a more uniform and concentrated emission.

The FEM images also reveal that the electron beams from uncoated CF and W emitters were unstable, with individual spots flickering in intensity and randomly switching on and off under applied voltage. This instability is attributed to the adsorption of residual gas contaminants on the uncoated emitter surfaces, which reduces both emission concentration and stability. In contrast, the FEM images of the PS-coated CF and W emitters show a more concentrated and stable beam. Consequently, the FEM images appear significantly brighter and more focused for the coated emitters.

This enhancement can be attributed to the protective role of the PS coating, which shields the emitter surface from ionized gas bombardment and reduces surface adsorption. In doing so, the PS coating helps preserve the chemical structure of the emitter surface and improves emission stability [9, 19, 22–25].

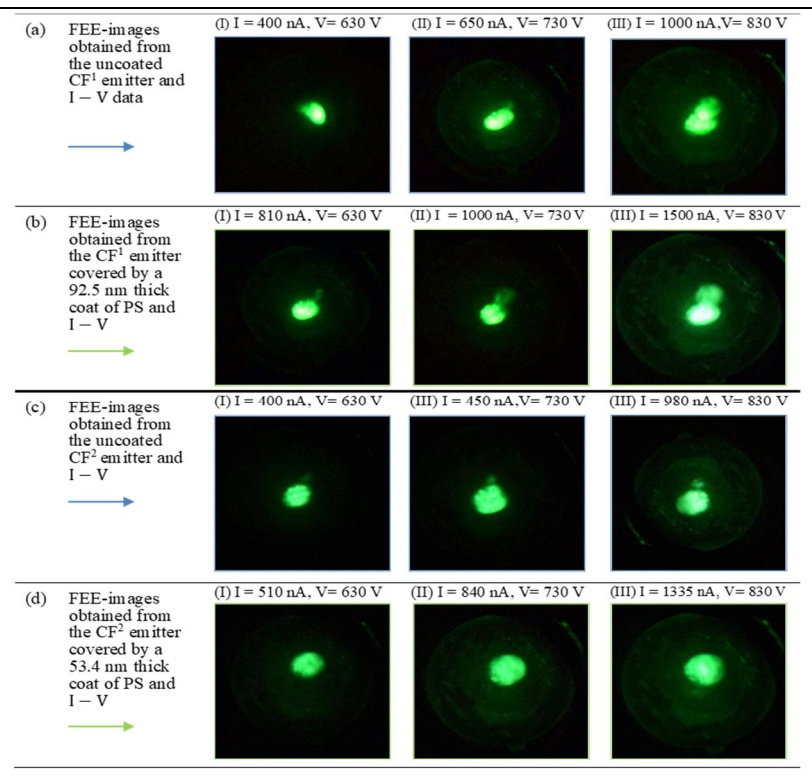


FIG. 13. Series of FEM images from CF¹ tips (a) uncoated and (b) coated with a 92.5 nm PS layer, and CF² tips (c) uncoated and (d) coated with a 53.4 nm PS layer. Spot size and brightness increase with applied voltage. All images were recorded under identical conditions: the same tip-to-screen distance and a 10-minute interval between exposures.

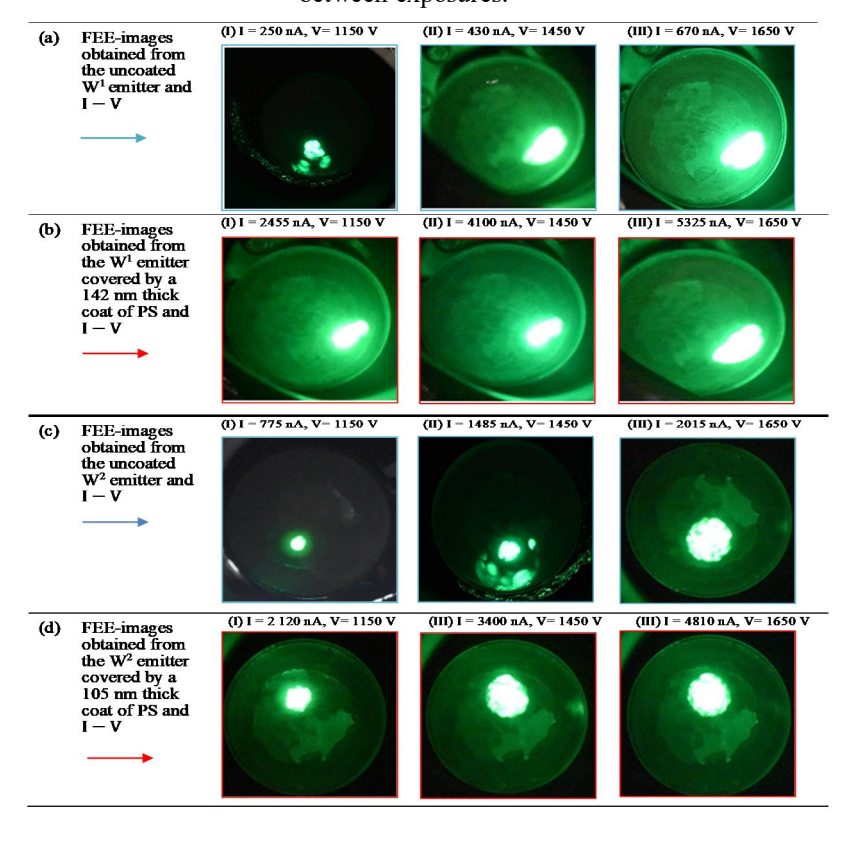


FIG. 14. Series of FEM images from W¹ tips (a) uncoated and (b) coated with a 142 nm PS layer, and W² tips (c) uncoated and (d) coated with a 105 nm PS layer. Spot size and brightness increase with applied voltage. All images were recorded under identical conditions: the same tip-to-screen distance and a 10-minute interval between exposures.

In general, when comparing the currentvoltage characteristic obtained from the two kinds of emitters, it is observed that the PS-coated CF and W emitters exhibit greater variation in their I - V curves compared to the uncoated ones. This variation stems from the PS-coated emitters' ability to emit at lower voltages with higher currents, indicating higher efficiency compared to the uncoated emitters. However, the impact of the PS coat on the FEE behavior differs between the two emitters, as evidenced by comparing the results before and after coating in Tables 1 and 2. Key agreements highlighting the contribution of the PS coating layer to the production of an improved, current-stabilized coated emitter include: (I) The PS coating layer improves the field electron emission initiation voltage for the coated emitter samples in both studies. This improvement manifests as a decrease in the starting voltage or an increase in the initial emission current, or both. (II) Additionally, the PS coating layer enhances the operating voltage range of the coated emitter during voltage increasing-and-decreasing cycles. This enhancement is characterized by starting at a lower voltage and reaching a higher voltage, and vice versa, thereby reducing the threshold voltage and increasing the operating voltage gap.

Coating both CF and W emitters with a PS layer proved highly beneficial, reducing the required supply voltage for emission initiation and yielding more condensed electron beams. However, marked differences were observed in the FEE characteristics of PS-coated CF and W emitters, evident from the results in Tables 1 and 2, including: (I) PS-coated W emitters exhibited a distinct 'switch-on' phenomenon. When the applied voltage was slowly increased, the emission current abruptly jumped from nearly zero to a large ISAT value. This behavior is attributed to PS optimizing the chemical structure of W, forming an effective composite that enables this effect. (II) Differences in sample geometry also contributed. Variations in radius and coating thickness, as measured from SEM images, affected the emission properties. PS-coated W emitters showed a larger built-in I - V hysteresis between the up and down cycles, requiring higher initiation and threshold voltages and operating over a wider voltage range than the coated CF emitters. (III) Murphy-Good plots of the current-voltage data revealed similar linearity in the low-field region for both coated CF and W emitters, but the slope for W was smaller.

This indicates greater stability and compatibility of W with the PS coating, improving performance in this region.

Figures 13 and 14 further demonstrate these differences. The PS-coated W emitters produced more concentrated beams than the PS-coated CF emitters, with FEM images showing brighter, more intense spots. This enhanced brightness is attributed to a combination of chemical structure, tip sharpness, and coating thickness. These factors not only increased the spot brightness of the PS-coated W samples but also contributed to higher emission current and overall stability.

In general, significant differences in the profiles and structures—size. shape, and chemical composition—were observed between uncoated and coated CF and W emitters. These differences directly influenced electron beam emission, resulting in variations in brightness [8, 16, 18, 23– 25, 28]. Both coated and uncoated emissions are governed by field electron emission theory and its associated models. For coated emitters, the emission process follows the metal-insulatorvacuum regime [12, 13, 21, 32]. In this regime, penetration of the electric field into the dielectric reduces the Schottky-Nordheim barrier, allowing electrons to tunnel from the metal substrate into the dielectric conduction band and then through the surface barrier into vacuum without thermal excitation [10, 11, 18, 20]. The sharpness of the emitter tip and the dielectric coating collectively lower the effective work function of the coated composite emitter. This ensures that even at relatively low extraction voltages, internal electrons can tunnel efficiently, producing higher emission currents. The work function of PScoated W emitters is lower than that of PS-coated CF emitters, leading to a more pronounced reduction of the potential barrier and improved emission characteristics. Consequently, the coated emitters deliver higher emission currents at lower extraction voltages. Furthermore, the stability and concentration of the electron beam from coated emitters are attributed to the field-induced formation of an emission channel through the dielectric layer at the emitter apex, concentrating the beam into a single bright spot. Differences in the composition structure of PS-coated CF and W samples could contribute to variations in the shape and size of the emission channel and, consequently, the concentration and beam stability [8, 9, 22, 23]. In summary, the coated composite emitter structure of the W sample

proves to be more suitable and stable, emitting a brighter, more intense, and more concentrated beam.

4. Conclusions

This work provides a brief analysis of two similar studies, highlighting their shared features and confirming the excellent field electron emission behavior of dielectric-coated emitter tips. Such emitters hold strong potential as advanced electronic field sources. From a technological standpoint, polystyrene-coated carbon fiber and tungsten emitters offer several advantages over uncoated emitters. Particularly noteworthy are their low operating voltages and high current values, enabling higher current densities for the same applied electric fields. Furthermore, polystyrene coating serves as a protective barrier, guarding the emission plane surface against undesired chemical or physical sorption of ions that could lead to tip bombardment. This protection allows the emitter to operate stably at lower vacuum levels compared to conventional field

emission emitters. Moreover, polystyrene coat significantly enhances concentration and stability of the emitted electron beam, resulting in more stable, concentrated, condensed, and brighter field-emission microscope current-distribution images compared to those obtained with uncoated emitters. Overall, the polystyrene coating layer, as demonstrated in both studies, leads to high source brightness, low emission threshold voltage, low operating voltage, and stable high emission current under high vacuum conditions. Polystyrene, as a coating material that yields enhanced results, stands as a viable option alongside epoxy resins and metal oxides for covering field electron emission emitter sources.

Acknowledgments

We acknowledge CzechNanoLab Research Infrastructure, supported by MEYS CR (LM2018110). Knápek and Allaham would like to acknowledge financial support from the Czech Academy of Sciences (RVO:68081731).

References

- [1] Baig, N., Kammakakam, I., and Falath, W., Mater. Adv., 2 (2021) 1821.
- [2] Khursheed, A., Ultramicroscopy, 128 (2013) 10.
- [3] Bronsgeest, M.S., Barth, J.E., Swanson, L.W., and Kruit, P., J. Vac. Sci. Technol. B, 26 (3) (2008) 955.
- [4] Swanson, L.W. and Schwind, G.A., "A Review of the Cold-Field Electron Cathode", In: "Advances in Imaging and Electron Physics", (Elsevier, 2009) pp. 63–100.
- [5] Lee, H.R., Lee, S.W., Shikili, C., Kang, J.S., Lee, J., and Park, K.C., J. Nanosci. Nanotechnol., 16 (2016) 12053.
- [6] Lei, W., Li, C., Cole, M.T., Qu, K., Ding, S., Zhang, Y., Warner, J.H., Zhang, X., Wang, B., and Milne, W.I., Carbon, 56 (2013) 255.
- [7] Nirantar, S., Ahmed, T., Bhaskaran, M., Han, J.-W., Walia, S., and Sriram, S., Adv. Intell. Syst., 1 (2019) 1900039.

- [8] Burda, D., Allaham, M.M., Knapek, A., Sobola, D., and Mousa, M.S., 2021 34th Int. Vacuum Nanoelectron. Conf., IVNC 2021. (2021).
- [9] Mousa, M.S., Knápek, A., and Grmela, L., Jordan J. Phys., 13 (2020) 171.
- [10] Mousa, M.S. and Kelly, T.F., Ultramicroscopy, 95 (2003) 125.
- [11] Mousa, M.S., Surf. Interface Anal., 39 (2007) 102.
- [12] Latham, R.V. and Mousa, M.S., J. Phys. D Appl. Phys., 19 (1986) 699.
- [13] Mousa, M.S., J. Phys. Colloques, 48 (1987) C6-109.
- [14] Miller, M.K., Kenik, E.A., Mousa, M.S., Russell, K.F., and Bryhan, A.J., Scr. Mater., 46 (2002) 299.
- [15] Mousa, M.S., Appl. Surf. Sci., 94–95 (1996) 129.
- [16] Allaham, M.M., Forbes, R.G., Knápek, A., Sobola, D., Burda, D., Sedlák, P., and Mousa, M.S., Mater. Today Commun., 31 (2022) 103654.

- [17] Forbes, R.G., R. Soc. Open. Sci., 6 (2019) 190912.
- [18] Knápek, A., Allaham, M.M., Burda, D., Sobola, D., Drozd, M., and Horáček, M., Mater. Today Commun., 34 (2023) 105270.
- [19] Knápek, A., Dallaev, R., Burda, D., Sobola, D., Allaham, M.M., Horáček, M., Kaspar, P., Matějka, M., and Mousa, M.S., Nanomaterials, 10 (2020) 1294.
- [20] Mousa, M.S. and Kelly, T.F., Surf. Interface Anal., 36 (2004) 444.
- [21] Mousa, M.S., Surf. Sci., 231 (1990) 142.
- [22] Al Soud, A., Knápek, A., and Mousa, M.S., Jordan J. Phys., 13 (2020) 191.
- [23] Al-Qudah, A.A., Mousa, M.S., and Fischer, A., IOP Conf. Ser. Mater. Sci. Eng., 92 (2015) 1.
- [24] Alnawasreh, S.S., Al-Qudah, A.M., Madanat, M.A., Ali, E.S.B., Almasri, A.M., and Mousa, M.S., Appl. Microsc., 46 (2016) 227.

- [25] Almarsi, A.M., Hagmann, M.J., and Mousa, M.S., Appl. Microsc., 47 (2017) 55.
- [26] Fawaeer, S.H., Shatnawi, M.T.M., Allaham, M.M., and Mousa, M.S., Adv. Mater. Process. Technol., 8 (2021) 2775.
- [27] Alabth, M., Shatnawi, M.T.M., Allaham, M.M., Burda, D., and Mousa, M.S., Ultramicroscopy, 244 (2023) 113643.
- [28] Madanat, M., Al Share, M., Allaham, M.M., and Mousa, M.S., J. Vac. Sci. Technol. B, 39 (2021) 024001.
- [29] Popov, E.O., Filippov, S.V., Kolosko, A.G., and Knápek, A., J. Vac. Sci. Technol. B, 40 (2022) 024201
- [30] Allaham, M.M., Forbes, R.G., and Mousa, M.S., Jordan J. Phys., 13 (2) (2020) 101.
- [31] Higashitani, K., Makino, H., and Matsusaka, S., "Powder Technology Handbook", 4th ed., (CRC Press, Boca Raton, FL: Taylor & Francis Group, LLC, 2019).
- [32] Mousa, M.S., J. Phys. Colloques, 48 (1987) C6-115.